
INFLUENCE OF GEOMAGNETIC DISTURBANCES ON SCINTILLATIONS OF GLONASS AND GPS SIGNALS AS OBSERVED ON THE KOLA PENINSULA

V.B. Belakhovsky

*Polar geophysical institute,
Apatity, Russia, belakhov@mail.ru*

P.A. Budnikov

*E.K. Federov Institute of Applied Geophysics,
Moscow, Russia, pavel9860@gmail.com*

A.S. Kalishin

*Arctic and Antarctic Research Institute,
St. Petersburg, Russia,
askalishin@aari.ru*

S.V. Pilgaev

*Polar geophysical institute,
Apatity, Russia, pilgaev@pgia.ru*

A.V. Roldugin

*Polar geophysical institute,
Apatity, Russia, roldugin_a@pgia.ru*

Abstract. We have compared effects of geomagnetic disturbances during magnetic storms of various types (CME and CIR) and during an isolated substorm on scintillations of GLONASS and GPS signals, using a Septentrio PolaRx5 receiver installed in Apatity (Murmansk Region, Russia). We analyze observational data for 2021. The magnetic storms of November 3–4, 2021 and October 11–12, 2021 are examined in detail. The November 3–4, 2021 magnetic storm was one of the most powerful in recent years. The analysis shows that the scintillation phase index reaches its highest values during nighttime and evening substorms ($\sigma_{\phi} \approx 1.5\text{--}1.8$), accompanied by a negative bay in the magnetic field. During magnetic storms, positive bays in the magnetic field, associated with an increase in the eastward electrojet, lead, however, to quite comparable values of the phase scintillation index.

An increase in phase scintillations during nighttime and evening disturbances correlates with an increase in the intensity of ULF waves (Pi3/Pc5 pulsations) and with the appearance of aurora arcs. This confirms the important role of ULF waves in forming the auroral arc and in developing ionospheric irregularities. The

predominance of the green line in the spectrum of auroras indicates the contribution of disturbances in the ionospheric E layer to the scintillation increase. Pulsating auroras, associated with ionospheric disturbances in the D layer, do not lead to a noticeable increase in phase scintillations. Analysis of ionospheric critical frequencies according to ionosonde data from the Lovozero Hydrometeorological Station indicates the contribution of the sporadic E_s layer of the ionosphere to jumps in phase scintillations.

The difference between phase scintillation values on GLONASS and GPS satellites during individual disturbances can be as great as 1.5 times, which may be due to different orbits of the satellites. At the same time, the level of GLONASS/GPS scintillations at the L2 frequency is higher than at the L1 frequency. We did not find an increase in the amplitude index of scintillations during the events considered.

Keywords: ionosphere, GLONASS, GPS, magnetic storm, substorm, aurora.

INTRODUCTION

High-latitude and polar ionospheric disturbances affect radio wave propagation in different frequency bands. Transionospheric decimetric signals used in Global Navigation Satellite Systems (GNSS) are also affected by high-latitude ionospheric disturbances. Irregularities in ionospheric plasma density distribution (with scales of the order of the first Fresnel zone, 100–300 m for GNSS) can lead to fast GNSS signal amplitude and phase fluctuations, known as ionospheric scintillations [Yeh, Liu, 1982; Basu et al., 2002]. Strong scintillations reduce the signal quality and even cause signal loss. The scintillation level is characterized by phase (σ_{ϕ}) and amplitude (S_4) scintillation indices. Amplitude scintillations are produced by plasma irregularities with scales from tens to hundreds of meters; and phase scintillations, by irregularities with scales from hundreds of meters to several kilometers.

Ionospheric scintillations are most pronounced in the equatorial region and at high latitudes [Basu et al., 2002, Kintner et al., 2007].

The rate of the total electronic content (TEC) ROT of the ionosphere is also utilized as a characteristic of GNSS signal disturbance. The fluctuation intensity was estimated using ROT -index ($ROTI$) maps for a high-latitude region [Cherniak et al., 2014]. TEC variations (ROT) are generally well related to the variations of σ_{ϕ} [Makarevich et al., 2021], yet during individual events this relationship may not be so obvious [Belakhovsky et al., 2021].

It is interesting to compare the level of fluctuations of signals from various satellite systems, namely, GLONASS and GPS, during geomagnetic disturbances. The American GPS system consists of 32 satellites with an orbital height of 20200 km and

an orbital inclination of 55° . The frequencies used are $L1=1575.42$ MHz, $L2=1227.60$ MHz. The Russian system GLONASS consists of 24 satellites with an orbital height of 19100 km and an orbital inclination of 64.8° . The frequencies used are $L1=1602$ MHz, $L2=1246$ MHz. Thus, due to the greater inclination of the orbit, GLONASS is better suited for monitoring the high-latitude ionosphere than GPS. Yasyukevich et al. [2017] have shown that the density of slips in pseudorange $P1$ measurements at high latitudes for GLONASS is lower than for GPS. At midlatitudes, on the contrary, the stability in measuring pseudorange at the fundamental frequency for GPS is higher than for GLONASS. In [Zakharov et al., 2016, 2020; Chernyshov et al., 2020], it has been demonstrated that the probability of a phase slip at $L2$, even under quiet conditions, is 3 to 15 times higher than at $L1$. A similar ratio is true of the slip probabilities for $P2$ and $P1$. At the same time, the probability of phase slips at $L2$ is higher than at $L1$ to ~ 10 times for G3-class magnetic storms and substorms. As the storm intensity increases, this ratio decreases to 5–7 times.

The auroral oval is characterized by a high level of ionospheric plasma turbulence. For example, most slips when determining TEC during geomagnetic storms occur near the auroral oval [Astafyeva et al., 2014]. It has been shown that the dynamics of the auroral oval (NORUSKA model) and the dynamics of the spatio-temporal distribution of TEC fluctuations, caused by ionospheric irregularities in the auroral oval region, are similar [Chernous et al., 2018]. There is a close correspondence between positions of the auroral oval and the oval of irregularities. The existing discrepancy may be due to the fact that the auroral oval is projected onto a height of 110 km; and the oval of irregularities, onto a height of 450 km, with no regard for the curvature of magnetic field lines. Chernous et al. [2015] have found that auroral arcs are indicators of disruptions in the operation of navigation systems. Shagimuratov et al. [2021] have shown that TEC fluctuations driven by auroras lead to positioning errors of more than 20 m when a signal passes through an auroral arc. Kozelov et al. [2019] have suggested that the interference in the GPS navigation of NATO forces during the Trident Juncture exercise in October–November 2018 might have been caused by space weather disturbances and auroral disturbances in the ionosphere.

There exist recurrent and non-recurrent magnetic storms. The former are associated with the appearance of coronal holes on the solar surface. They occur every 27 days, which corresponds to the solar rotation period. Recurrent storms are generated by corotating interaction regions (CIRs) created by high-speed solar wind (SW) streams flowing out of coronal holes [Gonzalez et al., 1994]. Recurrent magnetic storms are often called CIR storms. Non-recurrent storms do not have a strict periodicity in their occurrence, coronal mass ejections (CMEs) are responsible for them; therefore, they are called CME storms. Unlike CIR storms, CME storms are accompanied by the occurrence of a storm sudden

commencement (SSC) impulse, associated with the arrival of an interplanetary shock wave (ISW). Borovsky, Denton [2006] have identified 21 differences between CME and CIR magnetic storms.

The geomagnetic substorm is the most powerful disturbance at high latitudes. Magnetospheric substorms are a sequence of processes occurring after the period of southward interplanetary magnetic field (IMF) and leading to release of accumulated energy from the magnetotail. During substorms, the configurations of the magnetospheric and polar ionospheric current systems are disrupted, the geomagnetic field is dipolarized, energetic particles are injected into the geostationary orbit, $Pi2$ oscillations occur in the magnetic field, etc. [Kokubun et al., 1977]. Smith et al. [2008] have assumed that a discrete aurora is necessary for the occurrence of powerful phase GPS scintillations during substorms. Along with the scintillations, other effects were observed during auroras, such as signal loss [Prikryl et al., 2010].

In a series of recent papers [Belakhovsky et al., 2020, 2021; Belakhovsky et al., 2022], we have examined the effect of polar ionospheric disturbances on GPS signal scintillations from observations in the Svalbard archipelago, using data from the EISCAT 42m radar. A comparison was made between GPS signal scintillation effects due to precipitation in the cusp region, dawn precipitation, substorm precipitation, polar cap patches, precipitation during ISW arrival. Among the ionospheric disturbances of the types considered, substorms were shown to provide the highest σ_ϕ . At different times, the Svalbard archipelago is located near the polar boundary of the auroral oval, in the vicinity of the cusp, in the polar cap region. In this work, we use GNSS observations made on the Kola Peninsula, which on average is located in the more equatorial part of the auroral oval.

We examine the effect of ionospheric disturbances on GLONASS and GPS satellite signal scintillations for the auroral region, using observations made on the Kola Peninsula during magnetic storms of different types (CME and CIR) and during an isolated substorm.

1. DATA

We have used data from a Septentrio PolRx5 GNSS receiver, installed on the roof of the building of the Polar Geophysical Institute (Apatity) at the end of 2020. Geographic and geomagnetic coordinates of Apatity (APT) are 67.58° N, 33.31° E and 63.86° N, 112.9° E. The Septentrio PolRx5 GNSS receiver belongs to Federov Institute of Applied Geophysics (Moscow). We have analyzed the results of observations for 2021.

The scintillation GNSS receiver automatically calculates the phase σ_F and amplitude $S4$ scintillation indices, as well as ionospheric TEC for GPS, GLONASS, Galileo, and BeiDou satellites. The phase index is the standard deviation of the carrier wave phase, from which a low-frequency trend at 0.1 Hz is subtracted using a sixth-order Butterworth filter; the amplitude index is the standard deviation of the received signal power at 50 Hz, normalized to the average power

value in a 1-min window; ROT (the rate of TEC) is the first time derivative of TEC .

Optical observations of auroras based on data from the all-sky camera at PGI Lovozero Observatory were also used to identify ionospheric disturbances. To detect geomagnetic disturbances, we have taken data from a PGI magnetometer at Lovozero Observatory (LOZ), whose geographic and geomagnetic coordinates are 67.97° N, 35.02° E and 64.22° N, 114.6° E. For the analysis, we have also used maps of equivalent ionospheric current systems, constructed from IMAGE magnetometer network data.

We have employed the Canadian Advanced Digital Ionosonde (CADI) [Gao, MacDougall, 1991], installed at the Lovozero Hydrometeorological Station (HMS). The sounding is carried out in a frequency band 1–13 MHz; the peak transmission power does not exceed 600 W. The sounding signal is a 13-bit Barker code sequence with a four-cycle base pulse. The antenna system of the complex consists of two orthogonally arranged broadband delta curtain arrays. One delta-shaped antenna is transmitting; the other is receiving.

We have used OMNI database data to define SW and IMF parameters; $SYM-H$, AE indices, to determine the level of geomagnetic activity.

2. ANALYSIS OF EVENTS

The paper is based on GNSS data from the Septentrio receiver in Apatity for 2021. Over the period of interest, few magnetic storms were registered. In this paper, we compare the level of scintillations of signals from the American system GPS and the Russian system GLONASS during the November 3–5, 2021 and October 11–12, 2021 geomagnetic storms, as well as during an isolated substorm.

2.1. Isolated substorm

As an example, we analyze the February 12, 2021 substorm. There were quiet geomagnetic conditions: the $SYM-H$ index was 10 nT; AE , ~ 500 nT. Four days before the event, there were also no disturbances in the $SYM-H$ (Dst) index. The SW velocity V was ~ 350 km/s. The southward turn of IMF B_z at 16 UT (not shown in Figures) triggered a substorm.

We have compared geomagnetic variations from LOZ magnetometer data with the σ_ϕ and S_4 indices determined from GPS and GLONASS data (Figure 1). The phase and amplitude scintillation indices for different GPS and GLONASS satellites flying in the field of view of the Septentrio GNSS receiver (Apatity) are shown in different colors.

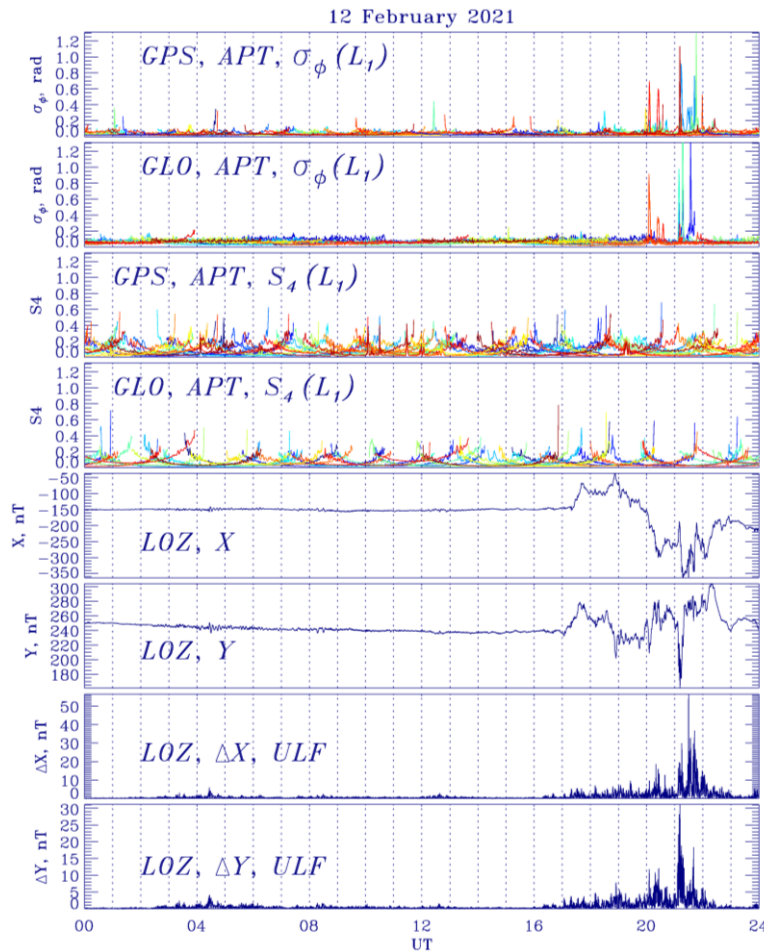


Figure 1. Phase scintillation index, amplitude scintillation index (at the L_1 frequency) as recorded by a receiver at the APT station (Apatity) for GPS and GLONASS satellites; geomagnetic field X-, Y-component variations according to Lovozero Observatory data; geomagnetic field X-, Y-component variations with a removed low-frequency trend (0.5 MHz) according to Lovozero Observatory data for February 12, 2021

The σ_ϕ index runs as high as 1.2–1.3 rad at 20–22 UT during the substorm (negative magnetic bay) associated with the development of a westward electrojet (see Figure 1). At the same time, σ_ϕ variations obtained from GPS and GLONASS satellite data are generally quite similar. There is no response in $S4$ during the disturbances considered.

To determine the contribution of ULF (ultralow-frequency) wave geomagnetic disturbances (Pc5/Pi3) to the scintillation increase, we subtracted the 0.5 MHz low-frequency trend from initial geomagnetic data (see Figure 1, two bottom panels). The bursts of ULF wave geomagnetic activity are seen to generally coincide with the σ_ϕ increase. This may suggest that ULF waves contribute to precipitation of charged particles (electrons, protons) into the high-latitude ionosphere. The charged particle precipitation produces ionospheric irregularities of various spatial scales, which leads to the occurrence of GNSS signal scintillations.

The largest increase in σ_ϕ was accompanied by the appearance of bright auroral arcs as derived from LOZ all-sky camera data (Figure 2) in the green line (557.7 nm). Green auroras are known to occur at ~ 100 – 120 km. We can therefore assume that the increase in phase scintillations was caused by ionospheric disturbances in the E-region.

Figure 3 shows diurnal variations in critical frequencies of the ionosphere as recorded by the LOZ HMS ionosonde (top panel); ionograms (two bottom panels). Here, f_oE_s is the critical frequency of the ionospheric E_s layer; $f_oE_{s\min}$ is the E_s -layer minimum critical frequency; f_oE is the E-layer critical frequency; f_oE_{\min} is the E-layer minimum critical frequency; f_oF2 is the F2-layer critical frequency; f_oF2_{\min} is the F2-layer minimum critical frequency; f_iE_s is the maximum reflected frequency from E_s . Analysis of the critical frequencies shows that the period 00–17 UT on February 12, 2021 had quiet conditions. Diurnal variations in the F2- and E-layer critical frequencies are clearly seen; minimum observed frequencies are within 1.3–1.7 MHz, which indicates the absence of absorption in the lower ionospheric layers. From 17 UT, minor ionospheric disturbances are recorded in the form of the sporadic layer E_s ; the critical value of f_oE_s ranges within 3.2–4 MHz. Ionospheric absorption increases slightly — the minimum observed frequencies are near 2 MHz. At 19:40 UT, there is a sharp increase in f_oE_s , as well as an

increase in f_iE_s — the maximum reflected frequency from E_s . In the ionograms, the E_s -region has a well-defined flat lower edge with fibrations and scattered reflections above it. Traces of the reflections from the E_s layer have a virtual height near 110–200 km. A similar structure of ionograms is usually observed during magnetic disturbances accompanied by auroras. From 20:10 to 21:35 UT, f_oE_s peaks and returns to the values before the explosive increase at 22:25 UT.

Comparison between σ_ϕ at $L1$ (see Figure 1) and at $L2$ (Figure 11, top panel) shows that σ_ϕ takes higher values at $L2$ than at $L1$ (see Figure 11). So, at 20–22 UT, σ_ϕ reaches values ~ 1.5 – 1.6 rad at $L2$ and ~ 1.2 – 1.3 rad at $L1$.

2.2. CME magnetic storm

We have analyzed the November 3–5, 2021 magnetic storm caused by the arrival of CME in Earth. Until recently, it was the strongest geomagnetic storm in the last 4.5 years; therefore, consideration of this event is of additional interest. The ISW arrival was detected at 22:00 UT as a sharp increase in the SW velocity and density, the IMF modulus, the $SYM-H$ index (Figure 4). The magnetic storm's intensity during the main phase was above average: $SYM-H \sim -120$ nT, $V \geq 800$ km/s, $AE \sim 3000$ nT. During the storm, the IMF B_z component changed its sign to negative (to -18 nT) several times, which led to penetration of SW plasma into Earth's magnetosphere.

According to LOZ data, the strongest substorm during this storm occurred on November 3 at 20–23 UT; its amplitude in the X component was ~ 1300 nT (Figure 5). Geomagnetic variations in the Y component during this substorm were ~ 500 nT (see Figure 5), which indicates the predominance of the auroral electrojet over vortex disturbances [Belakhovsky et al., 2023]. The substorm on November 4 at 00–03 UT had a lower intensity (700 nT).

Figure 5 compares effects of geomagnetic disturbances on GPS and GLONASS signals as derived from the Septentrio receiver data (Apatity). We compared GNSS scintillations with geomagnetic variations recorded at Lovozero Observatory. There was no noticeable increase in σ_ϕ during the SSC event ($\sigma_\phi \sim 0.1$ – 0.2 rad). The highest scintillation phase index ($\sigma_\phi \approx 1.8$ rad) determined by GPS and GLONASS satellites was observed during the substorm occurring after

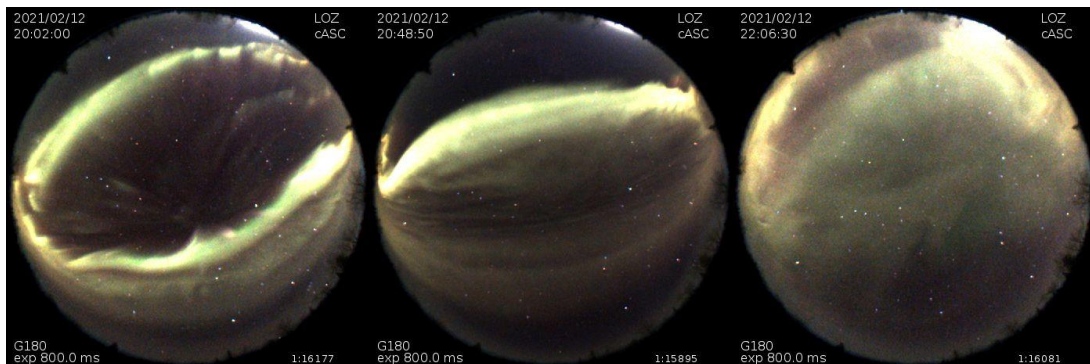


Figure 2. Frames from an all-sky camera at Lovozero Observatory for 20:02 UT, 20:48 UT, 21:09 UT on February 12, 2021

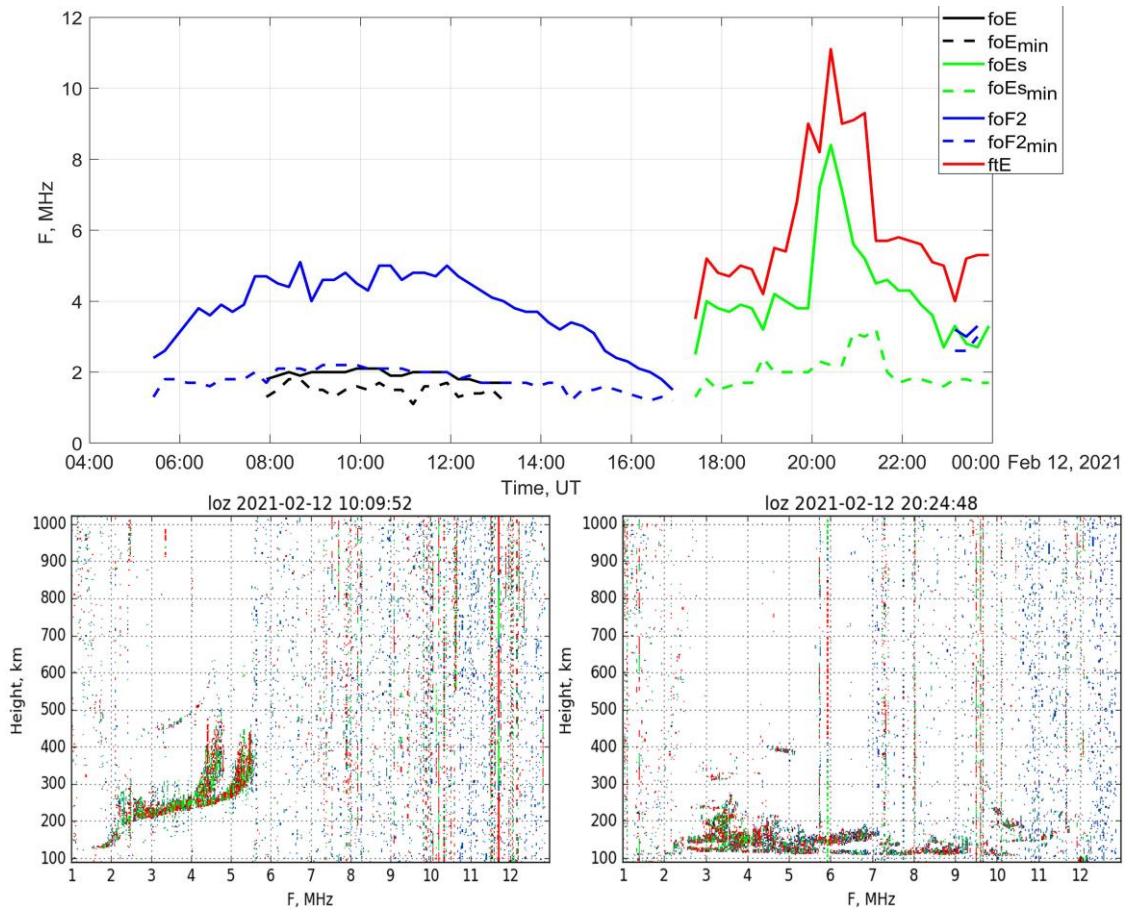


Figure 3. Diurnal variations in critical frequencies of the ionosphere; ionograms from the LOZ HMS ionosonde for February 12, 2021, 10:09 UT, 20:24 UT

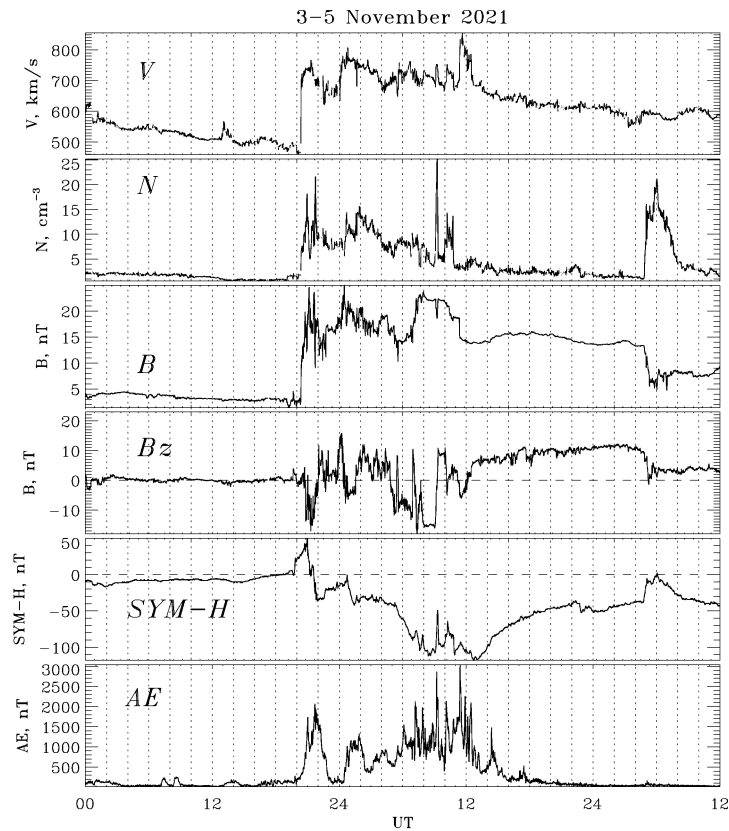


Figure 4. Variations in the solar wind velocity V , solar wind density N , IMF modulus B , IMF B_z component, $SYM-H$, AE on November 3–5, 2021

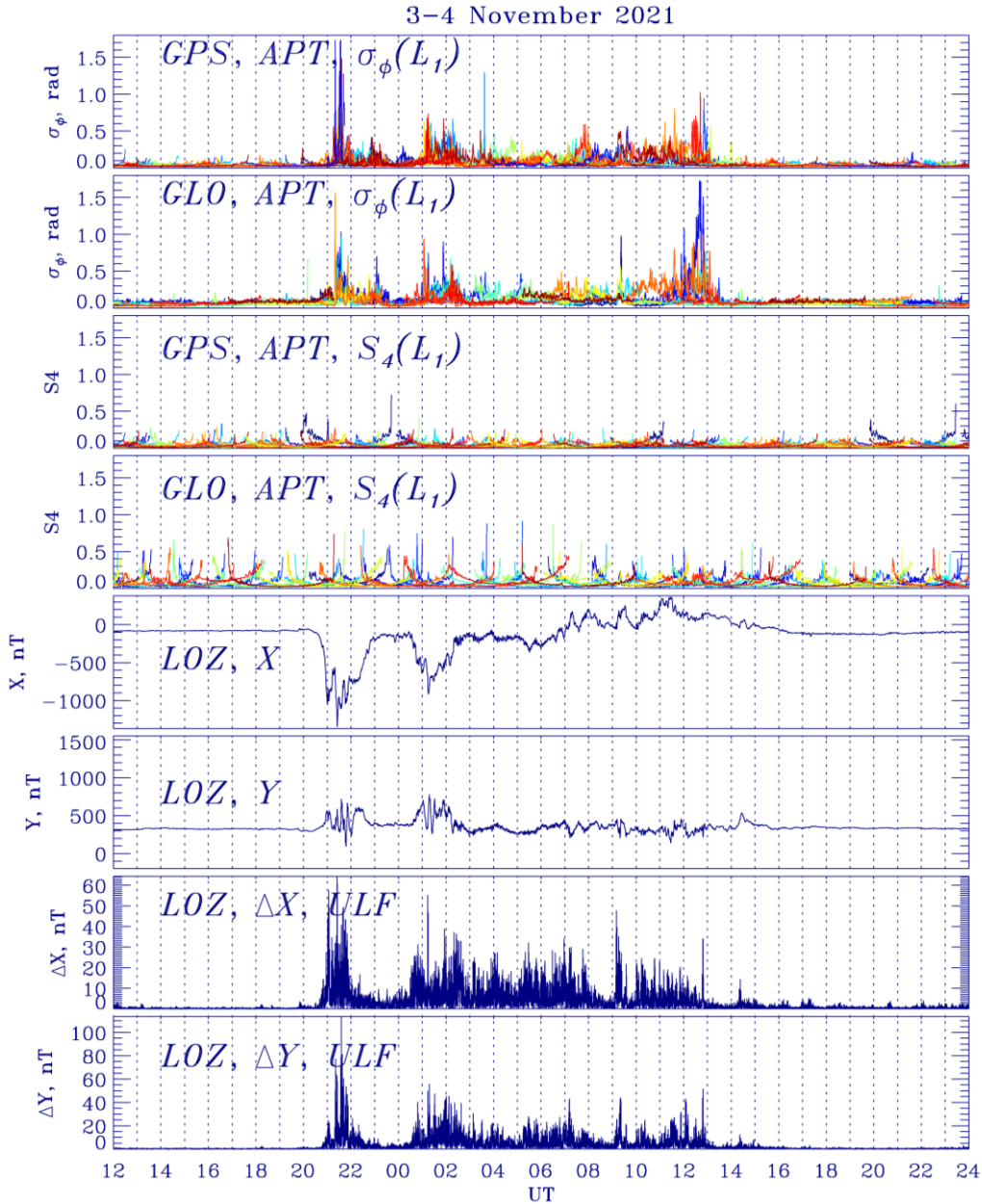


Figure 5. Phase scintillation index, amplitude scintillation index (at L1) recorded by a receiver at the APT station (Apatity) for GPS and GLONASS satellites; variations in the geomagnetic field X, Y components according to data from Lovozero Observatory; variations in the geomagnetic field X, Y components with a removed low-frequency trend (0.5 MHz) as derived from Lovozero Observatory data on November 3–4, 2021

the sudden magnetosphere compression (SSC event) on November 3, 2021 at 21–22 UT. The next substorm at 00–03 UT led to a lower level of phase scintillations (0.6–0.7 rad). High σ_ϕ values were observed not during the whole substorm, but only in its explosive phase. The ionospheric disturbances caused a noticeable increase in σ_ϕ not only in the nightside sector, but also in the dayside one during positive bays of the geomagnetic field. For example, an increase in phase scintillations was seen on November 4, 2021 at 12–14 UT ($\sigma_\phi \approx 1$ rad for GPS, $\sigma_\phi \approx 1.3$ rad for GLONASS).

Comparison between σ_ϕ values for GLONASS and GPS satellites shows that the difference may be almost 1.5 times. For example, during the substorm on November 3, 2021 at 21–22 UT, according to GLONASS data $\sigma_\phi \approx 1.2$ rad, and according to GPS data

$\sigma_\phi \approx 1.8$ rad. During the substorm on November 4, 2021 at 11–13 UT, according to GLONASS data $\sigma_\phi \approx 1.4$ rad; and according to GPS data, 1 rad.

The level of ULF oscillations (Pi3-Pc5 pulsations) was also determined by subtracting the low-frequency trend from the original signal (see the last two panels in Figure 5). ULF waves can contribute to the high level of GNSS scintillations since they are involved in precipitation of charged particles into the ionosphere, which lead to the development of ionospheric irregularities. There is a close relationship between the σ_ϕ increase and the increase in the amplitude of ULF oscillations during nighttime disturbances at 20–23, 00–04 UT. The ULF wave amplitude is as high as 120 nT for the Y component and 60 nT for the X component.

In the daytime sector (11–13 UT), no particular

connection was observed between the increase in σ_ϕ and the intensification of ULF waves. Presumably, other magnetospheric wave processes (VLF waves) contribute to the precipitation of charged particles into the atmosphere.

It was impossible to compare the sharp change in the value of σ_ϕ on November 3, 2021 at 21–22 UT with the behavior of critical frequencies of the ionosphere, using vertical sounding data, since there were no traces of reflections in the ionograms from 15:10 to 22:40 UT. Nonetheless, the σ_ϕ increase in the dayside sector from 12 to 13 UT on November 4 coincided well with the formation of a powerful sporadic E_s layer with a large number of off-angle reflections (Figure 6).

During this magnetic storm, the weather on the Kola Peninsula was cloudy, so there is no data on auroras for this event.

Comparison between σ_ϕ at L1 (see Figure 5) and L2 (Figure 11, middle panel) also shows that σ_ϕ takes higher values at L2 than at L1. At 20–22 UT, for example, σ_ϕ was as high as ~1.5–1.6 rad at L2 and ~1.2–1.3 rad at L1.

The S4 index of amplitude scintillations, determined by GPS and GLONASS satellites, was not perturbed during these disturbances.

2.3. CIR magnetic storm

We have analyzed the October 11–12, 2021 magnetic storm caused by the interaction between a high-speed SW stream from a coronal hole with a slower SW stream

(CIR). The intensity of the storm was moderate: $SYM-H \sim -72$ nT, $V \geq 500$ km/s, $AE \sim 2600$ nT (Figure 7). High variations in $SYM-H$ were generated by the change of IMF B_z to positive values.

According to LOZ magnetometer data (Figure 8), three geomagnetic substorms occurred sequentially: at 19–23, 23–02, and 02–05 UT. The third substorm ($\Delta X \sim 800$ nT) was the most intense; it was accompanied by a strong geomagnetic disturbance of the Y component ($\Delta Y \sim 700$ nT). During the first two substorms, the amplitude of geomagnetic disturbances in the X component was ~600–700 nT. During the third substorm, vortex current systems developed in the ionosphere [Belakhovsky et al., 2023].

All three substorms caused strong phase scintillations (Figure 8) for both GPS and GLONASS satellites ($\sigma_\phi \sim 1.5$ –2 rad). For this event, there was also a noticeable increase in σ_ϕ not only in the nightside sector, but also in the dayside one on October 12, 2021 at 14–16 UT ($\sigma_\phi \sim 1.5$ rad for GPS, $\sigma_\phi \sim 1.5$ –2 rad for GLONASS). The σ_ϕ increase in the dayside sector is due to a positive bay in the magnetic field ($\Delta X = 200$ nT).

The analysis shows that the increase in σ_ϕ is generally connected with the geomagnetic disturbance amplitude. For individual disturbances, however, a weaker geomagnetic disturbance can lead to larger σ_ϕ . For example, the magnetic substorm with an amplitude of ~600 nT (X component) on October 11 at 20–21 UT caused a more noticeable increase in phase scintillations

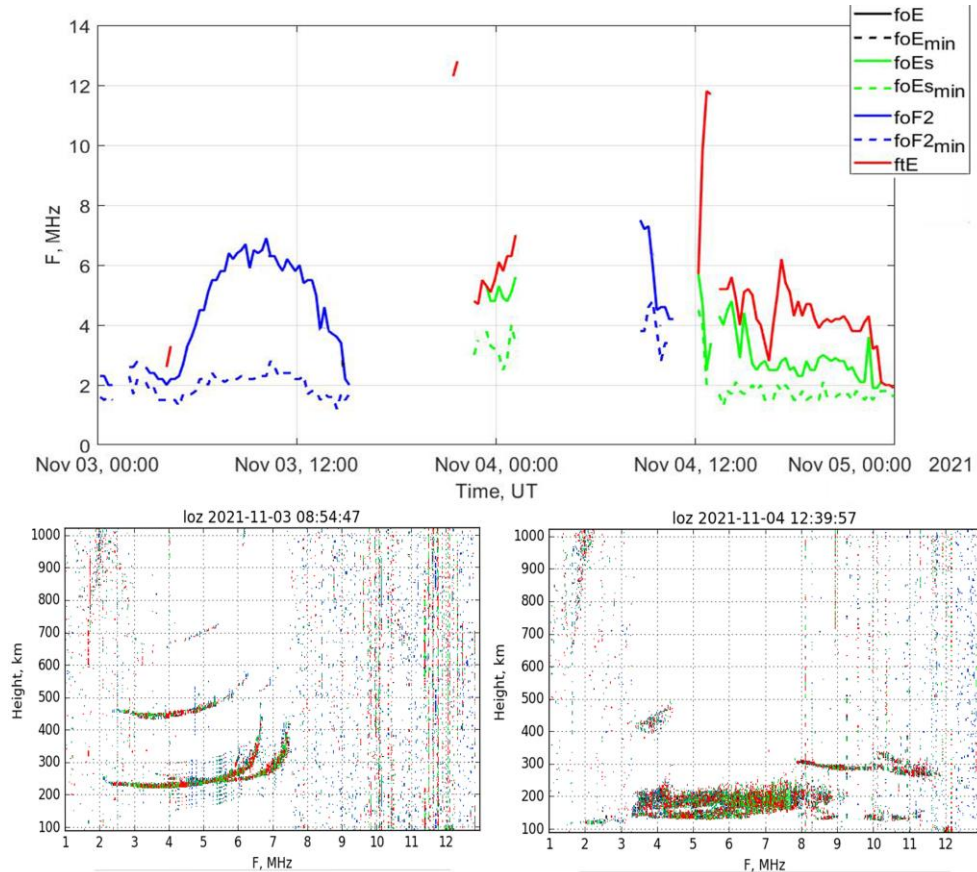


Figure 6. Diurnal variation in critical frequencies of the ionosphere on November 3–4, 2021; ionograms from the LOZ HMS ionosonde for November 03, 2021, 08:54 UT, and November 04, 2021, 12:39 UT

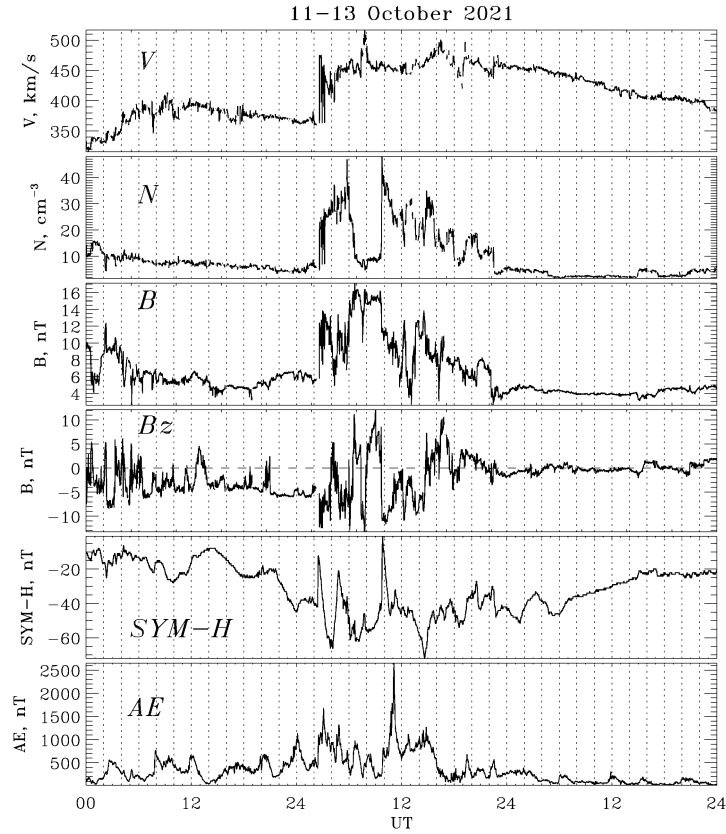


Figure 7. Variations in the solar wind velocity V , solar wind density N , IMF modulus B , IMF B_z , $SYM-H$, AE on October 11–13, 2021

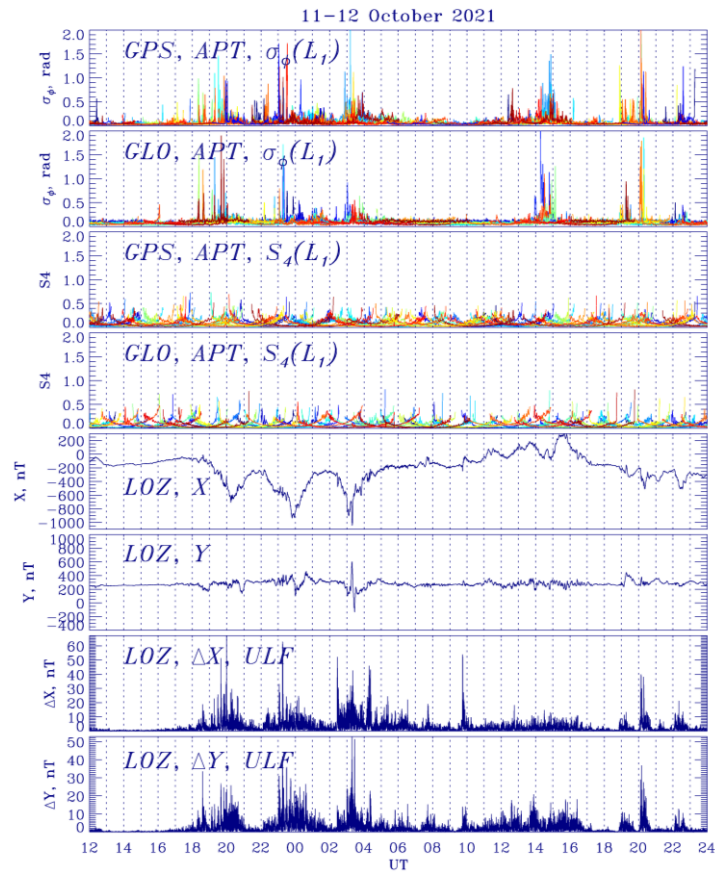


Figure 8. Phase scintillation index, amplitude scintillation index (at L_1) as recorded by the receiver at the APT station (Apatity) for GPS and GLONASS satellites; variations in the geomagnetic field X , Y components as observed by Lovozero Observatory; variations in the geomagnetic field X , Y components with a removed low-frequency trend (0.5 MHz) according to LOZ data for October 11–12, 2021

($\sigma_\phi \approx 2$ rad) than the substorm with 800–900 nT amplitude ($\sigma_\phi \approx 1.5$ rad) on October 12 at 03–04 UT.

The most powerful bursts of σ_ϕ are accompanied by the appearance of auroral arcs, as derived from the LOZ all-sky camera data (Figure 9, left and right panels, 19:39 and 23:17 UT). The predominance of the green line in the aurora spectrum indicates that the disturbances in the E layer contribute to the increase in σ_ϕ .

At the same time, pulsating auroras, characterized by a diffuse shape, are not accompanied by an increase in σ_ϕ (Figure 9, middle panel, 20:40 UT). The red emission during the occurrence of pulsating auroras is caused by the glow of molecular nitrogen N_2 at altitudes around 90 km.

The increase in σ_ϕ is connected with an increase in the ULF-wave amplitude (see Figure 8, two bottom panels) in the night and dusk sectors. ULF waves can lead to precipitation of auroral particles, which cause irregularities in the distribution of ionospheric plasma. The ULF-wave amplitude was as high as 50–60 nT for the X and Y components. But some jumps in σ_ϕ in the dayside sector (14–16 UT) do not correlate with the increase in the ULF-wave amplitude. Other wave processes in the magnetosphere (for example, VLF waves) in the dayside sector are likely to be responsible for the precipitation of charged particles into the atmosphere, increases in ionospheric disturbances and GNSS signal scintillations.

Analysis of vertical sounding ionograms at LOZ HMS (Figure 10) during the development of the most powerful phase scintillations indicates that the E_s layer is formed during an increase in σ_ϕ . The ionograms show intense lateral reflections from irregularities in the E_s -region; it has a well-defined flat lower edge with stratification and scattered reflections above it. A similar structure of ionograms is observed during magnetic disturbances followed by auroras. On October 11–12, ionospheric conditions were disturbed. During the daytime on October 11, the diurnal variation in the F2-layer critical frequency occurred; traces of reflections from the layer had type-F scattering. The minimum observed frequencies are near 3 MHz, which indicates high absorption. In the evening, there was an intense sporadic E_s layer. The increase in the critical frequency and the maximum reflected frequencies of the E_s layer (see Figure 10) during the first two substorms at 19–23 and 23–02 UT correlates well with σ_ϕ . During the strongest disturbance on October 12 from 02 to 05 UT, a complete absorption of sounding signals occurred and there were no traces of reflections in the ionograms. No traces of reflections from ionospheric layers are observed on October 12 till 12 UT. From 14 UT, intense E_s with many off-angle reflections is seen; increases in f_oF_2 and f_iE from 14 to 15 UT coincide with increases in the ULF-wave amplitude and σ_ϕ .

There is some difference in the level of σ_ϕ for GLONASS and GPS satellites (see Figure 8) both in one direction and in the other. For instance, during the substorm on October 12, 2021 at 02–04 UT, σ_ϕ according to GLONASS data was ~ 0.8 rad; and according to GPS data, 1–2 rad. During the substorm on October 11, 2021 at 18–21 UT, σ_ϕ according to GPS data was 1.4 rad; and according to GLONASS data, ~ 1.9 rad.

The level of σ_ϕ determined at L2 (Figure 11, bottom panel) is slightly higher than σ_ϕ at L1 (see Figure 8). At L2, σ_ϕ at some moments is as high as 2–2.5 rad; and at L1, $\sigma_\phi < 2$ rad.

There is no response of the amplitude scintillation index S_4 to the geomagnetic disturbances considered.

DISCUSSION

In this paper, we have analyzed GLONASS and GPS signal scintillations from observations on the Kola Peninsula, which is mostly located in the equatorial part of the auroral oval. Earlier in [Van der Meer et al., 2015; Oksavik et al., 2015], the levels of GPS and GLONASS signal scintillations were compared using a receiver in the Svalbard archipelago. It has been shown that σ_ϕ has fairly close values for GPS and GLONASS satellites during substorm disturbances and polar cap patches. The Svalbard archipelago is located more poleward of the auroral oval, the cusp or polar cap can also be projected there. For the equatorial part of the auroral oval, such a comparison has been made for the first time. For the more equatorial part of the auroral oval, such a comparison is quite relevant since there is a sufficiently developed infrastructure here and the negative impact of space weather factors can be significant.

It should also be emphasized that, as far as we know from the literature, this work is probably one of the few where the level of GNSS signal scintillations is analyzed using a set of ground instruments located in the high-latitude region of the Russian Federation (Kola Peninsula). The geophysical equipment we work with (the Septentrio GNSS receiver, the CADI ionosonde) was produced abroad.

In this paper, we have compared the level of phase scintillations during magnetic CME and CIR storms. In general, the analysis shows that during the CIR storm, which had a noticeably lower intensity, the level of phase scintillations has comparable and even greater values than during the CME storm ($\sigma_\phi \approx 1.8$ rad). Edemskiy, Yasyukevich [2022] have examined a parameter similar to σ_ϕ *ROTI*. They compared *ROTI* fluctuations during CME storms and high speed streams (*HSS*) in the auroral oval from *ROTI* keograms, constructed using data from GPS-receiver networks. The analysis showed that the highest *ROTI* values were observed during the storm main phase, with CME storms leading to higher *ROTI* than *HSS*. Therefore, the two events of CME and CIR storms we analyze in this paper are most likely to stand out somewhat from the general statistics.

The November 3–4, 2021 CME storm and the October 11–13, 2021 CIR storm have been compared in terms of another space weather factor — geomagnetically induced currents (*GIC*) — in [Belakhovsky et al., 2023]. It has been shown that a CIR storm leads to higher *GIT* values (almost twice) than a CME storm. Such a difference in *GIC* was attributed to the development of vortex-current systems in the ionosphere. This means that the CIR storm should be taken into account in terms of various space weather effects: an increase in *GIC* and ionospheric scintillations.

A noticeable difference in the level of phase scintillations according to GLONASS and GPS data in some cases may be due to different satellite orbits and the passage of signals through local ionospheric disturbances along different trajectories. We think that the difference in the level of phase scintillations for GPS and GLONASS satellites is unlikely to be due to the difference in the frequencies of signals from these systems since the $L1$ frequencies on GPS and GLONASS satellites are quite close (for GPS $L1=1575.42$ MHz, for GLONASS $L1=1602$ MHz). At the same time, in some cases the scintillation level is higher for GLONASS; in other cases, for GPS. The difference between $L1$ and $L2$ is much larger than that between $L1$ in GPS and GLONASS. However, the level of scintillations at $L2$ in all the cases considered

exceeds the level of scintillations at $L1$ by $\sim 20\%$.

Our analysis shows that the scintillation level for GLONASS and GPS satellites is higher at $L2$ for the events considered than at $L1$. This result checks well with those obtained earlier in [Zakharov et al., 2016; Chernyshov et al., 2020]. The statistical analysis of GPS signals for 2010–2014 for IGS and CHAIN network stations, located in the Arctic region (north of 55° N), has shown that the probability of phase slips at $L2$ is almost 10 times greater than at $L1$ for G3-class magnetic storms and substorms. As the storm intensity increases, this ratio decreases somewhat — to 5–7 times. Similar relations are obtained for the probabilities of slips in pseudorange.

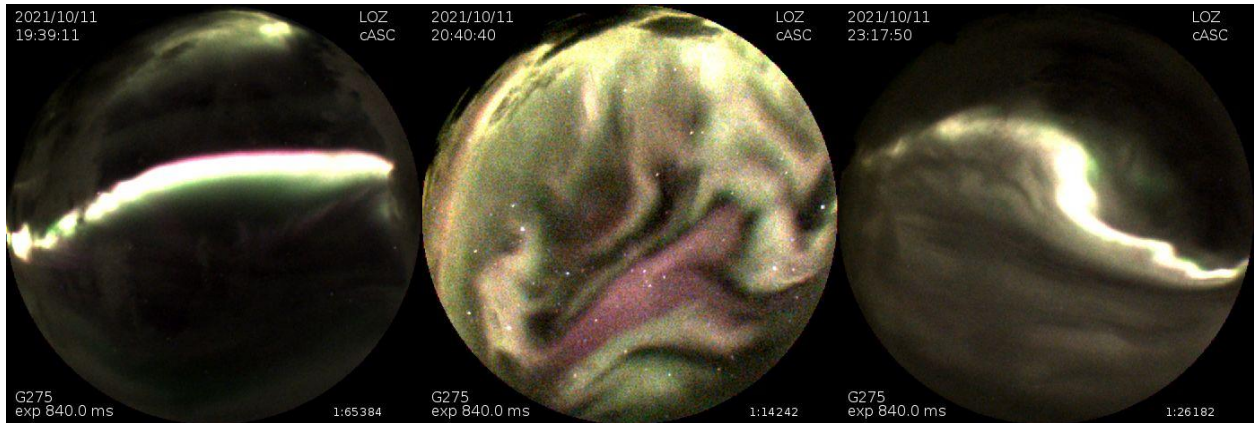


Figure 9. Frames from the all-sky camera at Lovozero Observatory for 19:39 UT, 20:40 UT, 23:17 UT on October 11, 2021

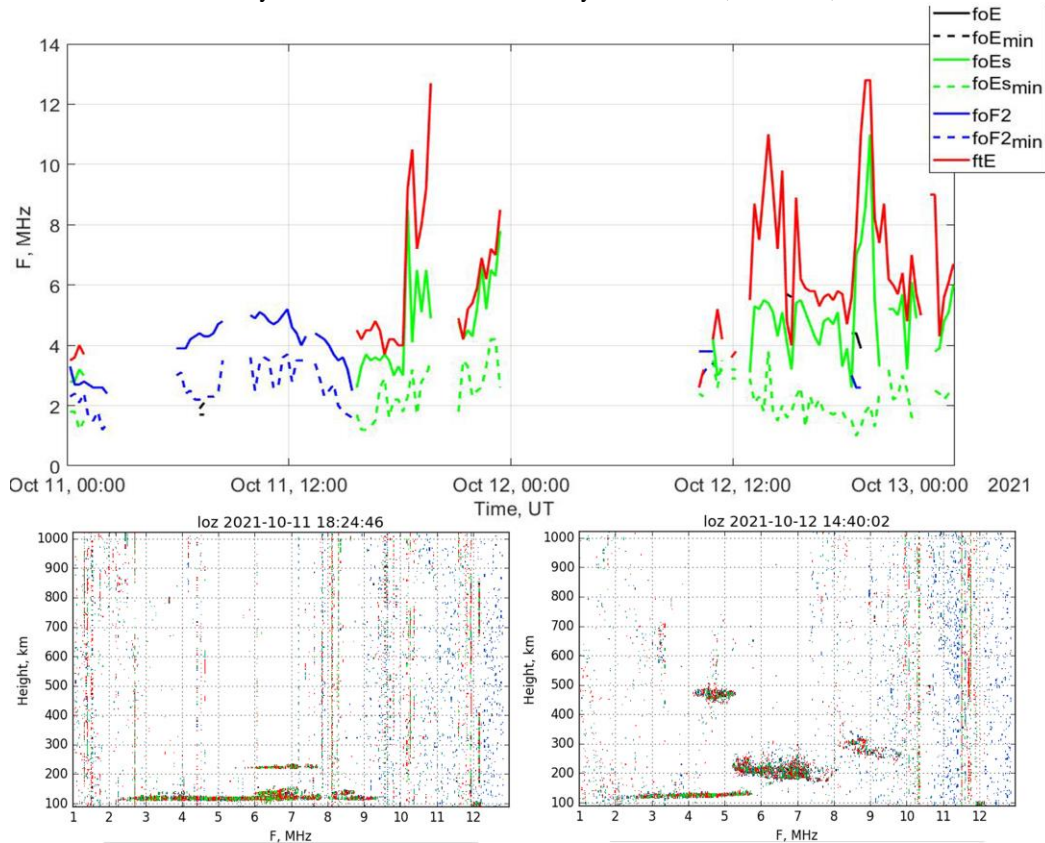


Figure 10. Diurnal variation in ionospheric critical frequencies on October 11–12, 2021; ionograms from the LOZ HMS ionosonde for October 11, 2021, 18:24 UT, and October 12, 2021, 14:40 UT

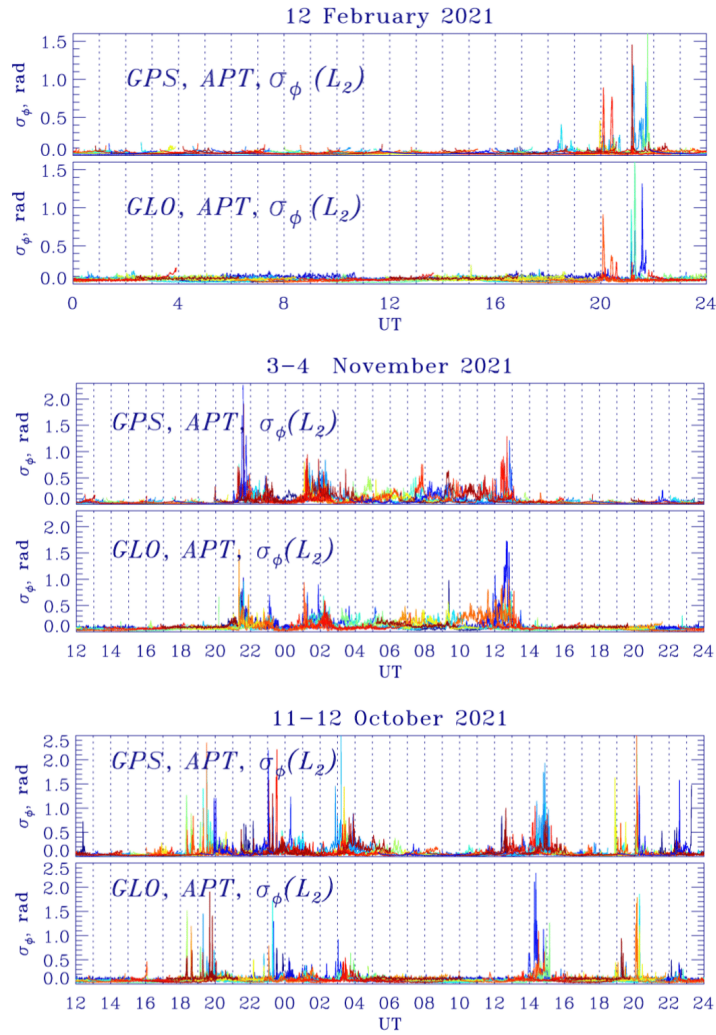


Figure 11. Variations in the phase scintillation index at L_2 for GPS/GLONASS satellites on February 12, 2021, November 3–4, 2021, and October 11–12, 2021

Our analysis shows that the largest increase in σ_ϕ for the events considered occurs during the substorm explosive phase. Comparison between the level of phase scintillations and the dynamics of auroras has revealed that discrete shapes of auroras (arcs, bands) are accompanied by the highest σ_ϕ . The predominance of bright discrete auroral shapes in the green line (557.7 nm) recorded by the all-sky camera at Lovozero Observatory during events with high σ_ϕ allows us to conclude that disturbances in the E layer make the greatest contribution to the increase in scintillations. The absence of bright auroras in the red line (630.0 nm) above 200 km during the appearance of the discrete shapes indicates the absence of strong disturbances in the F-region.

At the same time, pulsating auroras observed during the recovery phase of geomagnetic disturbances, as was shown for the October 11–12, 2021 CIR storm, do not cause a noticeable increase in σ_ϕ . It is believed that pulsating auroras are caused by precipitation of more energetic electrons of relativistic (subrelativistic) energies into the atmosphere [Miyoshi et al., 2015]. Thus, ionization of the D layer by high-energy electrons does not lead to a noticeable increase in GNSS scintillations.

Analysis of these ionograms confirms the formation of an E_s layer during the strongest scintillations. It should be said here that the ionosonde data were not available for all σ_ϕ jumps owing to absorption of radio waves emitted by the ionosonde at high ionization of the ionosphere. The analysis suggests that an increase in the critical frequency and maximum reflected frequencies of the E_s layer correlates with σ_ϕ . Of course, when an ionosonde signal is reflected from the E_s layer, there are no disturbances in the F-region. Nonetheless, the combination of ionosonde data with optical data on auroras (the predominance of the green line) allows us to conclude that disturbances in the E-region make the greatest contribution to the increase in phase scintillations. This is consistent with the results obtained in [Belakhovsky et al., 2021; Makarevich et al., 2021].

Indeed, the use of incoherent scattering radar would allow a more detailed analysis of the contribution of ionospheric layers to the scintillation increase. Unfortunately, there are no radars of this class at high latitudes on the territory of the Russian Federation. EISCAT incoherent scatter radars in Tromsø (ULF, VLF), located at ~630 km from Apatity, could provide indirect evidence about the contribution of ionospheric disturbances to the GNSS scintillation increase. But the

EISCAT radar works rather irregularly due to the high cost of such measurements, and in 2021 there were no suitable cases with EISCAT data in Tromsø. Earlier in [Makarevich et al., 2021; Belakhovsky et al., 2021] using incoherent scatter radars EISCAT 42m and PFISR, it has been shown that ionospheric disturbances in the E layer cause much more significant phase scintillations than disturbances in the F layer.

Previously, many papers [Smith et al., 2008; Prikryl et al., 2010] have examined the increase in phase GPS scintillations during the negative magnetic bay associated with the development of the westward electrojet. Indeed, analysis of the data for 2021 has shown that in most cases phase scintillations increase during nighttime geomagnetic disturbances. However, during magnetic storms, positive magnetic bays associated with enhancement of the eastward electrojet [D'Onofrio et al., 2014] lead to a quite comparable increase in phase scintillations. This should be taken into account when estimating the impact of space weather on navigation and communication systems at high latitudes.

Comparison of phase scintillations with geomagnetic ULF (Pc5/Pi3) wave activity has shown their close relationship for night and evening disturbances. There is no such clear relationship for dayside ULF disturbances. In the dayside sector, magnetospheric wave disturbances of other types (VLF waves) are most likely to also cause charged particles to precipitate into the ionosphere [Thorne et al., 2010]. The relationship of an increase in ULF waves with an increase in ionospheric scintillations and with the occurrence of auroral arcs may indicate a significant contribution of ULF waves, excited by field line resonance (FLR) inside the magnetosphere, to precipitation of charged particles into the atmosphere and to the formation of auroral arcs [Lyatsky et al., 1999; Belakhovsky et al., 2016].

The arrival of ISW in Earth's magnetosphere is accompanied by an SC impulse (SI) and can cause a series of phenomena in the magnetosphere and ionosphere [Belakhovsky et al., 2017]. However, the November 3–4, 2021 magnetic storm considered shows that the SSC impulse did not cause a noticeable increase in phase and amplitude scintillations of GLONASS and GPS signals. The ISW effect is likely to depend on a set of conditions, including local time.

There is a view that the absence of response of the amplitude scintillation index to geomagnetic disturbances of various types may be due to the peculiarities of calculating the indices for the high-latitude ionosphere. The software modules of GNSS scintillation receivers employ a standard method to calculate scintillation indices. To subtract the low-frequency trend associated with the motion of a satellite relative to a receiver, a lower filtering frequency of 0.1 Hz is used. The high-latitude ionosphere is characterized by high ionospheric convection velocity (100–1500 m/s), which also contributes greatly to signal refraction. In particular, this can result in high σ_ϕ in the absence of amplitude scintillations of disturbances (“phase without amplitude scintillations”) [Forte, 2005; Mushini et al., 2012]. To avoid this effect, it is

necessary to select the optimum lower filtering frequency. Many researchers have created their own scintillation indices to solve this problem [Mushini et al., 2012; Forte, 2005].

CONCLUSION

In this paper, we have estimated the influence of geomagnetic and auroral disturbances on scintillations of GLONASS and GPS signals during an isolated substorm, as well as during magnetic CME and CIR storms, using the Septentrio PolaRx5 receiver in Apatity (Murmansk Region, Russia).

Analysis shows that the greatest increase in GLONASS/GPS phase scintillations ($\sigma_\phi \approx 2$) occurs during night and evening substorms accompanied by negative magnetic bays caused by the development of the westward electrojet. However, during magnetic storms, positive bays in the dayside sector due to the development of the eastward electrojet can lead to a quite comparable level of scintillations. The ISW arrival did not cause a noticeable increase in phase scintillations. During a CIR storm, despite its lower intensity, the level of phase scintillations has quite comparable and even greater values than that during a CME storm.

We have shown that the level of phase scintillations is connected with an increase in the ULF wave amplitude (Pi3/Pc5) in the night (dusk) sector and to the occurrence of auroral arcs. This confirms the important role of ULF waves in the formation of an auroral arc and in the development of ionospheric irregularities.

The predominance of the green line in the spectrum of auroras suggests that disturbances in the E layer of the ionosphere contribute to an increase in scintillations. Analysis of ionospheric critical frequencies based on data from the LOZ HMS vertical sounding ionosonde indicates that the sporadic E_s layer is formed during the greatest increase in the phase scintillation index, which allows us to conclude that the E_s layer contributes to an increase in phase scintillations. The analysis suggests that an increase in the critical frequency and maximum reflected frequencies of the E_s layer correlates with σ_ϕ .

Pulsating auroras generated by precipitation of electrons of subrelativistic (relativistic) energies and having diffuse shapes are not accompanied by a noticeable increase in phase scintillations, which may indicate the absence of contribution of disturbances in the D layer to an increase in phase scintillations.

A noticeable difference in the level of phase scintillations has been found from GLONASS and GPS data, which is probably due to different satellite orbits and the passage of signals through local ionospheric disturbances along different trajectories. Moreover, the level of GLONASS/GPS scintillations at L2 is slightly higher than at L1.

No increase in GPS/GLONASS amplitude scintillations was detected during the events under study.

The work was financially supported by the Russian Science Foundation (Grant No. 18-77-10018 (Belakhovsky V.B.)).

REFERENCES

- Astafyeva E., Yasyukevich Yu., Maksikov A., Zhivetiev I. Geomagnetic storms, super-storms, and their impacts on GPS-based navigation systems. *Space Weather*. 2014, vol. 12, iss. 7, pp. 508–525. DOI: 10.1002/2014SW001072.
- Basu S., Groves K.M., Basu S., Sultan P.J. Specification and forecasting of scintillations in communication/navigation links: Current status and future plans. *J. Atmos. Solar-Terr. Phys.* 2002, vol. 64 (16), pp. 1745–1754.
- Belakhovsky V.B., Pilipenko V.A., Samsonov S.N., Lorentsen D. Features of Pc5 pulsations in the geomagnetic field, auroral luminosity, and riometer absorption. *Geomagnetism and Aeronomy*. 2016, vol. 56, iss. 1, pp. 42–58. DOI: 10.1134/S001679321506002X.
- Belakhovsky V.B., Pilipenko V.A., Sakharov Ya.A., Lorentzen D.L., Samsonov S.N. Geomagnetic and ionospheric response to the interplanetary shock on January 24, 2012. *Earth, Planets and Space*. 2017, vol. 69, iss. 1, article id. #105, 25 p.
- Belakhovsky V.B., Jin Y., Miloch W. Influence of the substorm precipitation and polar cap patches on GPS signals at high latitudes. *Sovremennyye problemy distantsionnogo zondirovaniya Zemli iz kosmosa* [Current problems in remote sensing of the Earth from space]. 2020, vol. 17, no. 6, pp. 139–144. DOI: 10.21046/2070-7401-2020-17-6-139-144.
- Belakhovsky V.B., Jin Y., Miloch W.J. Influence of different types of ionospheric disturbances on GPS signals at polar latitudes. *Ann. Geophys.* 2021, vol. 39, pp. 687–700.
- Belakhovsky V.B., Jin Y., Miloch W. Dayside scintillations of GPS signals according to the observations on the Svalbard archipelago. *Bulletin of the Russian Academy of Sciences: Physics*. 2022, vol. 86, iss. 3, pp. 348–353. DOI: 10.3103/S1062873822030066.
- Belakhovsky V.B., Pilipenko V.A., Sakharov Ya.A., Selivanov V.N. The growth of geomagnetic-induced currents during geomagnetic storms caused by coronal mass ejection and high-speed solar wind stream in 2021. *Bulletin of the Russian Academy of Sciences: Physics* 2023, vol. 87, no. 2, pp. 236–242.
- Borovsky J.E., Denton M.H. Differences between CME-driven storms and CIR-driven storms. *J. Geophys. Res.* 2006, vol. 111, iss. A7, A07S08. DOI: 10.1029/2005JA011447.
- Cherniak I., Krankowski A., Zakharenkova I. Observation of the ionospheric irregularities over the Northern Hemisphere: Methodology and service. *Radio Sci.* 2014, vol. 49, pp. 653–662. DOI: 10.1002/2014RS005433.
- Chernous S.A., Shvets M.V., Filatov M.V., Shagimuratov I.I., Kalitenkov N.V. Studying navigation signal singularities during auroral disturbances. *Russian J. Physical Chemistry B*. 2015, vol. 9, iss. 5, pp. 778–784. DOI: 10.1134/S1990793115050188.
- Chernous S.A., Shagimuratov I.I., Ievenko I.B., Filatov M.V., Efishov I.I., Shvets M.V., Kalitenkov N.V. Auroral Perturbations as an Indicator of Ionosphere Impact on Navigation Signals. *Russian Journal of Physical Chemistry B*. 2018, vol. 12, iss. 3, pp. 562–567. DOI: 10.1134/S1990793118030065.
- Chernyshov A.A., Miloch, W.J., Jin Y., Zakharov V.I. Relationship between TEC jumps and auroral substorm in the high-latitude ionosphere. *Scientific Reports*. 2020, vol. 10, article id. 6363. DOI: 10.1038/s41598-020-63422-9.
- D’Onofrio M., Partamies N., Tanskanen E. Eastward electrojet enhancements during substorm activity. *J. Atmos. Solar-Terr. Phys.* 2014, vol. 119, pp. 129–137.
- Edemskiy I.K., Yasyukevich Y.V. Auroral Oval Boundary Dynamics on the Nature of Geomagnetic Storm. *Remote Sensing*. 2022, vol. 14, iss. 21, p. 5486. DOI: 10.3390/rs14215486.
- Forte B. Optimum detrending of raw GPS data for scintillation measurements at auroral latitudes. *J. Atmos. Solar-Terr. Phys.* 2005, vol. 67, pp. 1100–1109. DOI: 10.1016/j.jastp.2005.01.011.
- Gao S., MacDougall J. A dynamic ionosonde design using pulse coding. *Can. J. Phys.* 1991, vol. 68, p. 1184.
- Gonzalez W.D., Joselyn J.A., Kamide Y., Kroehl H.W., Rostoker G., Tsurutani B.T., Vasyliunas V.M. What is a geomagnetic storm? *J. Geophys. Res.* 1994, vol. 99, A4, pp. 5771–5792.
- Kintner P.M., Ledvina B.M., de Paula E.R. GPS and ionospheric scintillations. *Space Weather*. 2007, vol. 5, p. S0900.
- Kokubun S., McPherron R.L., Russell C.T. Triggering of substorms by solar wind discontinuities. *J. Geophys. Res.* 1977, vol. 82, pp. 74–86.
- Kozelov B.V., Chernous S.A., Shagimuratov I.I., Filatov M.V., Efishov I.I., Tepenitsina N.Yu., Fedorenko Yu.V., Pilgaev S.V. Heliogeophysical factors, the influence of which could cause errors in GPS operation during the NATO military exercises “Trident Juncture” from 25/10/2018 to 7/11/2018. *Physics of Auroral Phenomena, Proc. XLII Annual Seminar*. 2019, pp. 48–52. (In Russian).
- Lyatsky W., Elphinstone R.D., Pao Q., Cogger L.L. Field line resonance interference model for multiple auroral arc generation. *J. Geophys. Res.* 1999, vol. 104, iss. A1, pp. 263–268. DOI: 10.1029/1998JA900027.
- Makarevich R.A., Crowley G., Azeem I., Ngwira C., Forsythe V.V. Auroral E-region as a source region for ionospheric scintillation. *J. Geophys. Res.* 2021, vol. 126, p. e2021JA029212. DOI: 10.1029/2021JA029212.
- Mushini S.C., Jayachandran P.T., Langley R.B., MacDougall J.W., Pokhotelov D. Improved amplitude and phase-scintillation indices derived from wavelet detrended high-latitude GPS data. *GPS Solutions*. 2012, vol. 16, pp. 363–373. DOI: 10.1007/s10291-011-0238-4.
- Miyoshi Y., Oyama S., Saito S., Kurita S., Fujiwara H., Kataoka R., Ebihara Y., Kletzing C., Reeves G., Santolik O., Clilverd M., Rodger C.J., Turunen E., Tsuchiya F. Energetic electron precipitation associated with pulsating aurora: EISCAT and Van Allen Probe observations. *J. Geophys. Res.* 2015, vol. 120, pp. 2754–2766. DOI: 10.1002/2014JA020690.
- Oksavik K., Van der Meeren C., Lorentzen D.A., Baddeley L.J., Moen J. Scintillation and loss of signal lock from poleward moving auroral forms in the cusp ionosphere. *J. Geophys. Res.* 2015, vol. 120, pp. 9161–9175. DOI: 10.1002/2015JA021528.
- Prikryl P., Jayachandran P.T., Mushini S.C., Pokhotelov D., MacDougall J.W., Donovan E., Spanswick E., St-Maurice J.-P. GPS TEC, scintillation and cycle slips observed at high latitudes during solar minimum. *Ann. Geophys.* 2010, vol. 28, pp. 1307–1316.
- Shagimuratov I.I., Filatov M.V., Efishov I.I., Zakharenkova I.E., Tepenitsyna N.Y. Fluctuations in the total electron content and errors in GPS positioning caused by polar auroras during the auroral disturbance of September 27, 2019. *Bulletin of the Russian Academy of Sciences: Physics*. 2021, vol. 85 (3), pp. 318–323.
- Smith A.M., Mitchell C.N., Watson R.J., Meggs R.W., Kintner P.M., Kauristie K., Honary F. GPS scintillation in the high arctic associated with an auroral arc. *Space Weather*. 2008, vol. 6, p. s03d01. DOI: 10.1029/2007SW000349.
- Thorne R.M., Ni B., Tao X., Horne R.B., Meredith N.P. Scattering by chorus waves as the dominant cause of diffuse auroral precipitation. *Nature*. 2010, vol. 467, pp. 943–946. DOI: 10.1038/nature09467.
- Van der Meeren C., Oksavik K., Lorentzen D.A., Rietveld M.T., Clausen L.B.N. Severe and localized GNSS scintillation at the poleward edge of the nightside auroral oval during intense substorm aurora. *J. Geophys. Res.* 2015, vol. 120, iss. 12, p. 10607-10621.

Yasyukevich Yu.V., Zhivetiev I.V., Yasyukevich A.S., Voeykov S.V., Zakharov V.I., Perevalova N.P., Titkov N.N. Ionosphere and magnetosphere disturbance impact on operation slips of global navigation satellite systems. *Sovremennye problemy distantsionnogo zondirovaniya Zemli iz kosmosa* [Current problems in remote sensing of the Earth from space] 2017, vol. 14, no. 1, pp. 88–98. (In Russian).

Yeh K.C., Liu C.H. Radio wave scintillations in the ionosphere. *Proc. IEEE*. 1982, vol. 70, no. 4, pp. 24–64. DOI: 10.1109/PROC.1982.12313.

Zakharov V.I., Yasyukevich Yu.V., Titova M.A. Effect of magnetic storms and substorms on GPS slips at high latitudes. *Cosmic Res.* 2016, vol. 54, iss. 1, pp. 20–30. DOI: 10.1134/S0010952516010147.

Zakharov V.I., Chernyshov A.A., Miloch W., Jin Y. Influence of the ionosphere on the parameters of the GPS navigation signals during a geomagnetic substorm. *Geomagnetism and Aeronomy*. 2020, vol. 60, iss. 6, pp. 754–767. DOI: 10.1134/S0016793220060158.

Original Russian version: Belakhovsky V.B., Budnikov P.A., Kalishin A.S., Pilgaev S.V., Roldugin A.V., published in *Solnechno-zemnaya fizika*. 2023. Vol. 9. Iss. 3. P. 60–70. DOI: [10.12737/szf-93202307](https://doi.org/10.12737/szf-93202307). © 2023 INFRA-M Academic Publishing House (Nauchno-Izdatelskii Tsentr INFRA-M)

How to cite this article

Belakhovsky V.B., Budnikov P.A., Kalishin A.S., Pilgaev S.V., Roldugin A.V. Influence of geomagnetic disturbances on scintillations of GLONASS and GPS signals as observed on the Kola Peninsula. *Solar-Terrestrial Physics*. 2023. Vol. 9. Iss. 3. P. 54–67. DOI: [10.12737/stp-93202307](https://doi.org/10.12737/stp-93202307).